APPROXIMATE ANALYTICAL FRACTURE MECHANICS APPROACH TO THE DESIGN OF CONCRETE STRUCTURES

Alberto Carpinteri,
Dipartimento di Ingegneria Strutturale, Politecnico di Torino, Torino, Italy.
Roberta Massabó,
Istituto di Scienza delle Costruzioni, Universitá di Genova, Genova, Italy.

Abstract: A nonlinear fracture mechanics model is applied along with linear elastic fracture mechanics solutions to analyze the flexural behavior of different composite materials. A cracked cross section of a beam in bending is considered and the constitutive flexural relationship is evaluated, on varying the mechanical and geometrical properties. The influence of material composition on the structural behavior as well as the size–scale effects are studied.

1 Introduction

Cementitious materials, such as concrete or mortar, and fiber–reinforced cementitious materials are characterized by an internal crack controlling mechanism, exerted by the secondary phases, i.e., aggregates and fibers. The secondary phases bridge the macrocracks along their wake and the microcracks in the process zone ahead of the macrocracks, thus preventing their coalescence, opening and growth. The mechanical behavior of structural components, the type of response and the size–scale effects are controlled by the above mentioned bridging mechanisms.

Two analytical approaches, based on fracture mechanics concepts, are used to analyze the composite failure process: the bridged–crack model, which assumes a non–vanishing crack–tip stress intensity factor, and the cohesive–crack model, which assumes a vanishing stress intensity factor. Numerous theoretical models, derived from the models of Barenblatt (1959, 1962) and Dugdale (1960), have been proposed (Cox and Marshall 1994). Many of these are concerned with the flexural behavior of composites used in civil engineering applications, such as, concrete and mortar (Hillerborg et al. 1976, Jenq and Shah 1985, Shah 1988, Carpinteri 1989, Cotterel et al. 1992), fiber–reinforced cementitious materials (Wecharatana and Shah 1983, Visalvanich and Naaman 1983, Ballarini et al. 1984, Mai 1985, Jenq and Shah 1986, Foote et al. 1986, Li and Liang 1986, Hillerborg 1989, Carpinteri and Massabó 1995.a, b) and reinforced concrete (Romualdi and Batson 1963, Carpinteri 1984, Desay and Ganesan 1986, Bosco and Carpinteri 1992, Bosco and Carpinteri 1995).

In this paper a nonlinear fracture mechanics model, previously formulated by the authors for analysis of the flexural behavior of brittle–matrix composites (Carpinteri and Massabó, 1995.b), is applied along with Linear Elastic Fracture Mechanics (LEFM) solutions to analyze the influence of mechanical and geometrical properties on the constitutive flexural relationship of a composite beam. Different bridging mechanisms are examined and the predicted size–scale effects in the flexural response are explained. Numerical examples and simulations of experimental tests are also shown.

2 Theoretical model

The proposed theoretical model analyzes the evolution of crack propagation in a brittle–matrix composite cross section in bending. This defines the constitutive flexural relationship which links the applied moment M to the localized rotation ϕ. The scheme of Fig.1, representing the cracked cross section of a beam of depth h and thickness b, is considered. In accordance with the models of Barenblatt (1959, 1962) and Dugdale (1960), the crack of depth a consists of a traction–free part of depth a_r and a fictitious part of depth a_f, acted upon by closing tractions σ_0. The fictitious crack can represent either a microcracked process zone ahead of a macrocrack or a macrocrack wake bridged by reinforcing elements. The normalized crack depths $\xi = a/h$, $\xi_r = a_r/h$ and $\xi_f = a_f/h$ are defined together with the normalized value $\zeta = x/h$ of the generic coordinate x related to the bottom of the cross section.

The reinforcements are assumed to be uniformly distributed and are taken into account in the post–cracking loading phase through the closing tractions σ_0, which are linked to the crack profile $w(x)$, according to an assigned relationship $\sigma_0(w)$ (Fig.1). If the reinforcements are present in a low volume ratio, the pre–cracking response of the composite coincides with that of the matrix, which is assumed to be linear–elastic. Reference is made to the two–dimensional single–edge notched–strip solutions (Tada et al. 1985) to define the fracture mechanics parameters.

At the tip of the crack a global stress intensity factor K_I can be defined by means of the superposition principle:

$$K_I = K_{IM} - K_{I\sigma} \tag{1}$$

where K_{IM} and $K_{I\sigma}$ are the stress intensity factors due to the applied bending moment M and to a distribution of opening tractions σ_0, respectively. The minus sign on the right–hand side of eq.(1) accounts for the shielding effect exerted by the closing tractions on the crack tip stress intensification.

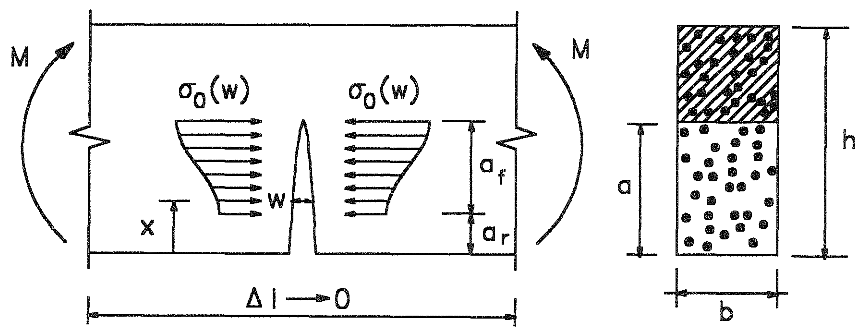

Fig.1: Schematic of the cracked cross section in bending.

Two different crack growth criteria are applied depending on the assumed crack tip stress field. If the matrix is brittle and K_{IC} is the fracture toughness, a singular stress field can be assumed and the crack starts propagating when K_I reaches the critical value K_{IC}. In this case the closing tractions (bridging tractions), which control crack opening, are governed by the properties of the reinforcing phase and by its interaction with the matrix.

On the other hand, a finite stress field can be assumed in the crack tip vicinity provided the closing tractions (cohesive tractions) represent the combined restraining action of the matrix and the secondary phases on crack propagation. In this case the crack propagates when the global crack tip stress intensity factor K_I vanishes, the matrix toughness being merged with the toughening mechanism of the secondary phases. The damage process producing the advancement of the crack is the same as that governing the opening process along the process zone.

By means of eq.1 and the assumed crack growth criterion the crack–propagation moment can be evaluated. In dimensionless form it is given by:

$$\frac{M_F}{K_{IC}h^{1.5}b} = \frac{1}{Y_M(\xi)}\left\{B\int_{\xi_r}^{\xi}\frac{\sigma(w(\zeta))}{\sigma_u}\,Y_P(\xi,\zeta)\,d\zeta + K\right\} \quad (2)$$

where $Y_M(\xi)$ and $Y_P(\xi,\zeta_i)$ are polynomial functions related to the shape of the specimen, and the parameters K and B characterize the crack tip stress field and the brittleness of the cross section, respectively.

On assuming a singular stress field at the tip of the crack, K_{IC} represents the matrix fracture toughness, K is equal to 1, σ_u is the ultimate strength of the reinforcements, or the maximum value of the bridging relation $\sigma(w)$, ρ is the fiber volume ratio, and $B{=}N_P{=}(\rho\sigma_u h^{0.5})/K_{IC}$ is the brittleness number, formerly proposed by Carpinteri (1984) for the description of the failure mechanisms in reinforced concrete. On assuming a finite stress field at the tip of the crack, K_{IC} represents the homogenized toughness of the composite, K is equal to 0, σ_u is the homogenized ultimate strength of the composite, or the maximum value of the cohesive relation $\sigma(w)$, and $B{=}1/s{=}(\sigma_u\ h^{0.5})/\ K_{IC}$ is the reciprocal of the brittleness number s originally defined by Carpinteri (1981) for the description of the failure mechanisms in brittle homogeneous materials.

The localized rotation ϕ for the crack at the onset of propagation can be calculated using the superposition principle and the localized compliances due to the crack. It is given by:

$$\begin{aligned}\phi = \frac{2K_{IC}}{Eh^{0.5}}\Bigg\{ & \frac{M_F}{K_{IC}h^{1.5}b}\int_0^{\xi} Y_M^2(\xi)\,d\xi\ + \\ & - B\int_{\xi_r}^{\xi}\left(\int_{\zeta}^{\xi} Y_M(y)Y_P(y,\zeta)\,dy\right)\frac{\sigma(w(\zeta))}{\sigma_u}\,d\zeta\Bigg\}.\end{aligned} \quad (3)$$

where E is Young's modulus of the composite. Eqs.(2) and (3) define a nonlinear statically indeterminate problem, the indeterminate closing tractions depending on the unknown crack opening displacements. A numerical iterative procedure has been formulated to evaluate the beam configuration satisfying equilibrium and compatibility (Carpinteri and Massabó 1995.a).

3 Constitutive flexural relationship

The shape of the constitutive flexural relationship of a brittle–matrix composite undergoes modifications when the mechanical and geometrical properties of the member are varied. Two different applications of the proposed model, which highlight different kinds of behavior of the member in flexure, are shown.

In the first case the stress field in the crack tip vicinity is assumed to be finite and the composite material is characterized by a linearly decreasing cohesive law, linking the closing traction to the crack opening displacement w. The cohesive relation $\sigma_0 = \sigma_u(1 - w/w_c)$ is assumed, w_c being the critical crack opening displacement beyond which the closing tractions vanish. The evolution of crack propagation in a cross section with an initial notch of depth $a_0 = 0.1h$ is analyzed.

In Fig.2 the dimensionless relationships relating the crack propagation moment $M_F/(K_{IC}h^{1.5}b)$ to the normalized rotation $(\phi E h^{0.5})/K_{IC}$, are shown. In accordance with the theoretical model proposed by Carpinteri and Massabó (1995.b), the flexural behavior is controlled by the dimensionless parameter s=$K_{IC}/(\sigma_u\, h^{0.5})$. The thin curves in the diagram relate to s=10.00, 5.00, 2.00, 1.00, 0.50 and 0.25. A transition from a strain–hardening behavior, for the greatest brittleness number s=10.00, to a to strain–softening behavior, for the lowest brittleness number s=0.25, is found. If the mechanical properties are kept unchanged, this transition is consequent to an increase in the beam depth. The theoretical model predicts a size–scale effect characterized by a *ductile* to *brittle* transition. This kind of behavior, typical of quasi–brittle materials, such as concrete, mortar or rocks, have been widely observed and theoretically reproduced (see, for instance, Carpinteri 1989).

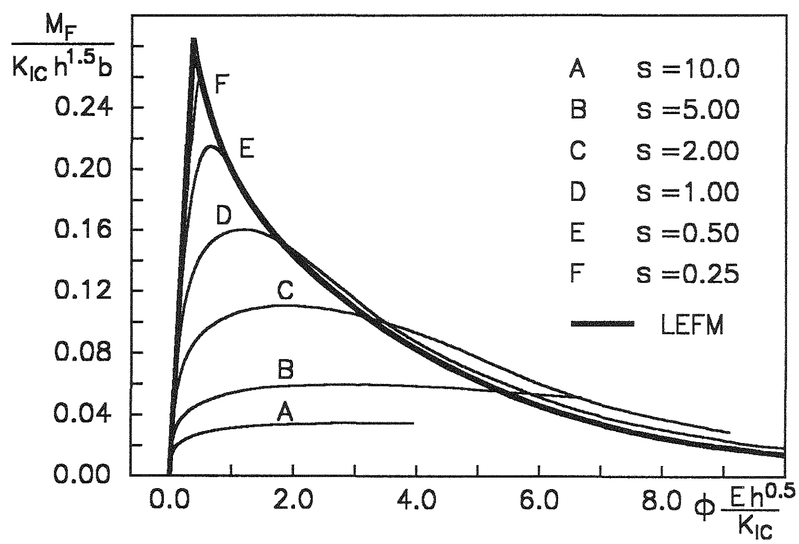

Fig.2: Relationships between the dimensionless moment and the normalized rotation for a composite characterized by a linearly decreasing cohesive law.

The thick curve shown in the diagram of Fig.2 has been evaluated based on the assumption of small–scale bridging, using LEFM solutions. The small–scale bridging condition for brittle–matrix composites assumes the existence of a process or bridging zone at the tip of the traction–free crack, which is small in relation to the crack size and the body dimensions. The diagram brings out the well–known result according to which the ultimate loading capacity of the cross section and the entire curve predicted by a cohesive–crack model, tend to the limit predicted by LEFM when the brittleness number s decreases (see curve F in Fig.2).

In Fig.2 it is also observed that, for decreasing values of s, the thin curves tend to draw nearer the LEFM curve after intersecting it. For brittleness numbers $s \leq 2$, the intersection points represent the beam configuration for which the traction–free crack starts propagating, and from that point on the LEFM macrostructural responses are almost coincident with the responses predicted by the cohesive option. On the other hand, the initial branches of the thin curves, as well as the peak values, differ from the ones predicted by LEFM, and are strongly dependent on both the brittleness number value and the shape of the assigned cohesive law. These branches reproduce the composite response during the loading phase in which the process zone is increasing and the shape of the crack faces is controlled by the cohesive tractions.

The diagrams of Fig.2 bring out that LEFM can be applied, with generic values of the brittleness number, for an approximate and conservative description of the constitutive branches beyond the intersection points. Application of LEFM to predict the tail of the constitutive flexural relationship considerably simplifies the calculations connected with the nonlinear integral problem of the cohesive crack model, which involve iterative numerical processes that encounter great difficulty in reaching convergence and require considerable mesh refinements whether for low brittleness numbers or for high crack depth values.

The second application of the theoretical model concerns a composite material characterized by a singular stress field at the crack tip and by a discontinuous bridging relationship, $\sigma(w)=\rho\sigma_u$ if $w \leq w_c$, and $\sigma_0(w)=0$ if $w > w_c$.

In this case the flexural behavior of the cross section is controlled by two dimensionless parameters, $N_P=\rho\sigma_u h^{0.5}/K_{IC}$ and $\tilde{E}\tilde{w}_c=(Ew_c)/(K_{IC}h^{0.5})$ (see Carpinteri and Massabó 1995.b). If only the size–scale effect is of interest, constant mechanical properties can be assumed. The product of the two dimensionless parameters, $N_P\tilde{E}\tilde{w}_c = (\rho\sigma_u Ew_c)/\ K_{IC}^2$, which does not depend on the depth of the cross section, is then fixed.

The dimensionless moment–vs.–localized rotation diagrams, $M_F/(K_{IC}h^{1.5}b)$ vs. $(\phi Eh^{0.5})/K_{IC}$, shown in Figs. 3, 4 and 5, relate to three different values of the parameter $N_P \tilde{E} \tilde{w}_c$, namely 36, 256 and 900. Beams with an initial matrix crack depth $a_0 = 0.1h$ crossed by unbroken fibers have been considered. The constitutive relationships have been evaluated by following the evolution of the crack up to $a = 0.9h$. In each diagram a series of curves, for brittleness numbers N_P varying from 0.1 to 2.1, is depicted. Since the mechanical properties are kept unchanged, these curves represent the responses of beams of different depths. In particular, an increase in N_P means an increase in the beam depth.

All of the curves in the diagrams of Figs. 4, 5 and 6 are characterized by three branches. The first is the linear–elastic branch describing the flexural response until the crack starts to propagate. The second branch depends on the brittleness number N_P and has been evaluated by applying the proposed model. It describes the beam behavior in large–scale bridging, namely when the bridging zone is invading the cross section and the crack is fully crossed by the fibers. The third unstable branch does not depend on the assumed brittleness number N_P, and has been evaluated using LEFM. It describes the behavior in small–scale bridging, when the traction–free crack propagates in the cross section. The small–scale bridging regime is controlled by the sole parameter $N_P \tilde{E} \tilde{w}_c$. As this parameter has been fixed for each figure, a single curve describes the third branch in all cases (see Carpinteri and Massabó, 1995.b).

Let us first consider the diagrams shown in Fig.4, which depict all of the probable behaviors. In the inset some curves are redrawn to highlight the variations in the structural response. The beam with N_P=0.5 shows a hyper–strength phenomenon, i.e. a peak loading capacity greater than the ultimate loading capacity at total disconnection. The response of this beam in the first post–cracking phase is strongly affected by the matrix fracture toughness, which prevails over the secondary phase toughening action controlling the ultimate loading capacity. The beam with N_P=1.1 shows a snap–through instability, which is an indication of an unstable crack advancement, arrested by the toughening action of the reinforcements. This instability would be represented by a jump at constant load if the process were controlled by the applied moment. After the discontinuity, the strain–hardening branch is controlled by the toughening action of the reinforcements which cross the crack up to total disconnection of the beam. The beam with N_P=2.1 reaches the third unstable branch, which results in a catastrophic crack propagation, before complete disconnection.

The global responses of the beams with $N_P = 0.5$, $N_P = 1.1$ and $N_P = 2.1$ are strain–softening, strain–hardening and strain–softening, respectively. This composite material is therefore characterized by a size–scale effect represented by a double transition

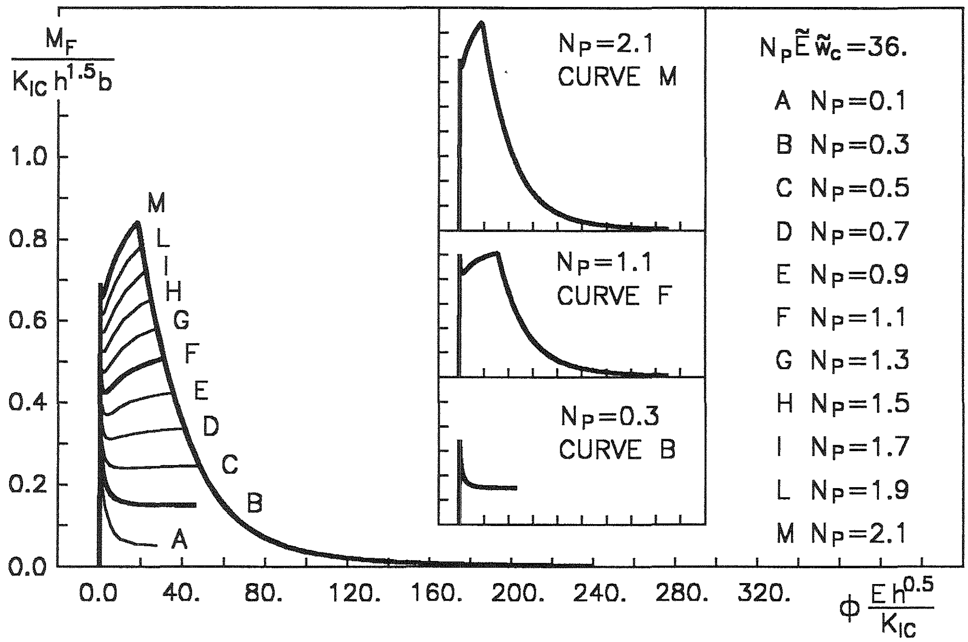

Fig.3: Dimensionless moment–vs.–rotation diagram for a composite characterized by a rectilinear bridging relation and $N_P \tilde{E} \tilde{w}_c = 36$.

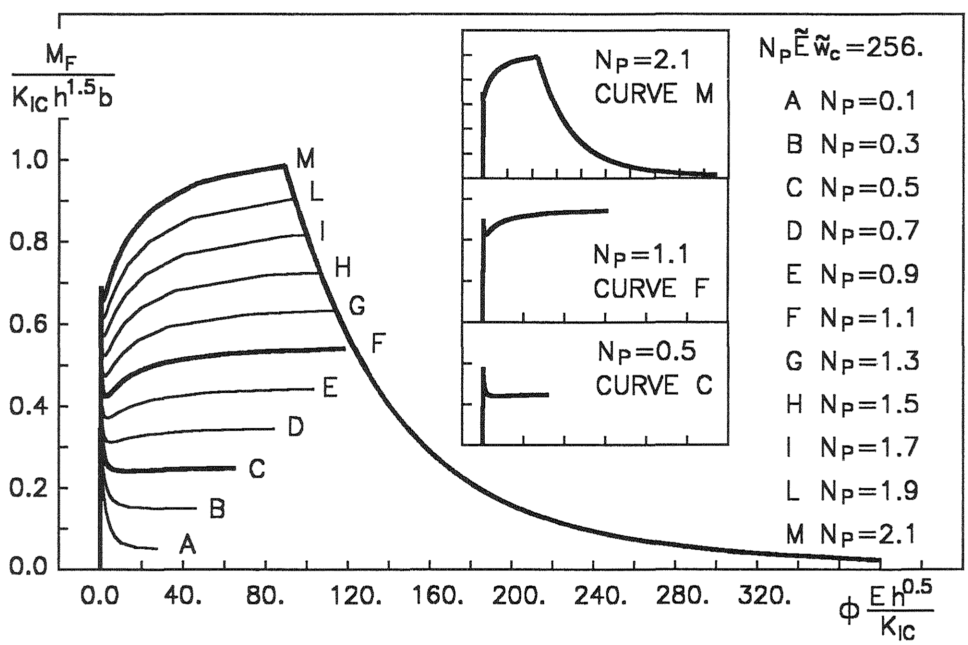

Fig.4: Dimensionless moment–vs.–rotation diagram for a composite characterized by a rectilinear bridging relation and $N_P \tilde{E} \tilde{w}_c = 256$.

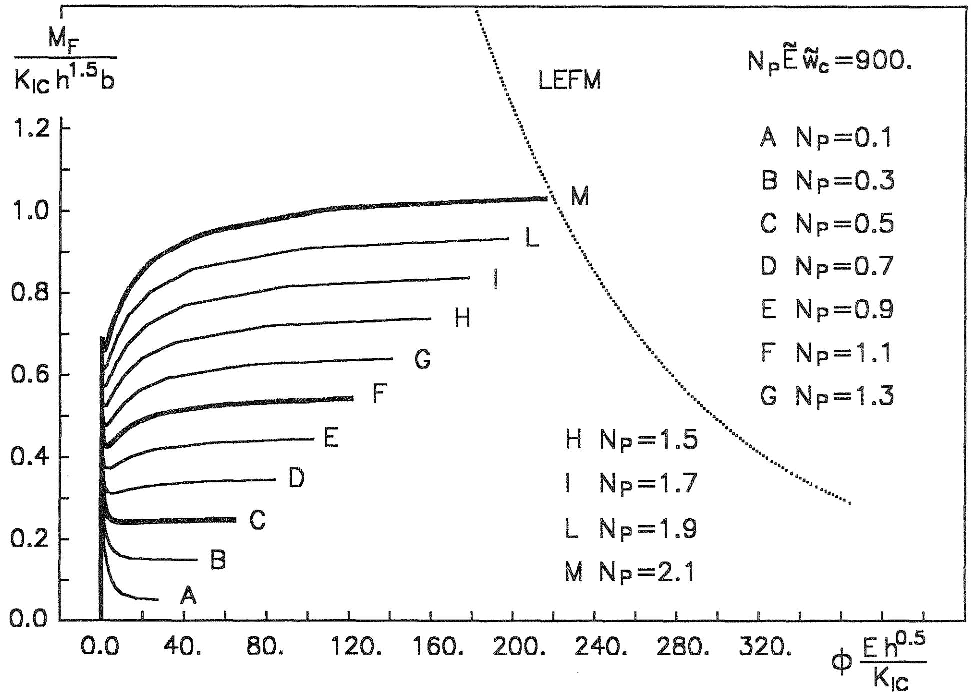

Fig.5: Dimensionless moment–vs.–rotation diagram for a composite characterized by a rectilinear bridging relation and $N_P \tilde{E} \tilde{w}_c = 900$.

in the flexural behavior, *brittle* to *ductile* and then the reversal *ductile* to *brittle*. To estimate the kind of effects the double transition can have on the design of the structural components, consider a steel fiber–reinforced cementitious material with K_{IC}=$50Nmm^{-1.5}$, E= 40000 Nmm^{-2}, ρ=0.02, σ_u=$200Nmm^{-2}$, and w_c=$4mm$. This results in a value of $N_P \tilde{E} \tilde{w}_c$ equal to 256. The curves in the inset of Fig.4 characterize the constitutive flexural behavior of three beams made of this composite, and of different depths, $h \simeq 40mm$, $h \simeq 190mm$ and $h \simeq 690mm$, respectively. The depths of the first two beams are in the range normally covered by the laboratory specimens and in this range a typical *brittle–ductile* transition is predicted when the beam depth increases. Experimental results of this kind have been obtained by Jamet et al. (1995) on fiber–reinforced concrete beams. However, in the steel fiber reinforced composite under consideration a new dangerous *ductile–brittle* transition is predicted when the beam depth is further increased. The largest beam considered, which could represent a real structural component, shows a strain–softening behavior.

When the mechanical properties of the beam are varied, the structural responses show substantial alterations. In the diagrams of Fig.3, obtained for the lowest value of $N_P \tilde{E} \tilde{w}_c$, strain–softening behavior is predicted for all brittleness numbers. The low value of $N_P \tilde{E} \tilde{w}_c$ may be due to a small critical crack opening displacement or to a low fiber volume ratio.

On the other hand, in the diagrams of Fig.5, obtained for a higher value of $N_P \tilde{E} \tilde{w}_c$, the structural responses vary from strain–softening to strain–hardening when the brittleness number increases, so that a *brittle–ductile* scaling transition is predicted. The LEFM curve, shown in the diagram of Fig.5, does not intersect the different curves obtained in large–scale bridging; for this reason, the second ductile–brittle transition, shown by the previously examined material, does not appear in the range of the brittleness numbers considered. The thick curves in Fig.5 represent, for instance, the behavior of a fiber–reinforced cementitious material with K_{IC}=$25 N/mm^{1.5}$, E=$40000 N/mm^2$, ρ=0.01, σ_u=200 N/mm^2, w_c=$7mm$ and beam depths of $h \simeq 40mm$, $h \simeq 190mm$ and $h \simeq 690mm$, respectively. The flexural responses in Fig.5 coincide with the ones of a composite reinforced with fibers characterized by a rigid–perfectly plastic bridging relationship, for which the brittleness number N_P is the single governing parameter.

It is worth noticing that the assumption of a different bridging law $\sigma_0(w)$ modifies the theoretical curves, generally giving rise to smoother responses and more complex trends of the branches preceding the intersection points with the LEFM solution.

In conclusion, the proposed theoretical model predicts that for each brittle–matrix composite material of known mechanical properties and bridging mechanism, there exists a critical beam depth (or a critical N_P) beyond which the flexural responses change from being globally stable to globally unstable. The existence of this critical value in the range of depths embracing the laboratory samples and the actual structural components, depends on the properties of the composite material and on the position assumed by the LEFM curve in the dimensionless moment vs. rotation diagram. It is therefore evident that the composition of the composite (kind of matrix and fibers and their volume ratio) can be suitably designed in order to avoid the dangerous ductile to brittle transition.

4 Applications

To verify the applicability of the proposed theoretical model some of the experimental tests carried out on fiber–reinforced mortar beams by Jenq and Shah (1986) have been simulated. The beams, loaded in a three–point bending scheme, have a depth × thickness × span of $76 \times 19 \times 280 mm$ and a notch of depth $a_0 \simeq 25mm$. The unreinforced matrix fracture toughness is equal to

K_{IC}=27.5$Nmm^{-1.5}$, and Young's modulus has been evaluated to be 22000Nmm^{-2}. Four different beams with fiber volume ratio equal to ρ=0.00, 0.005, 0.010 and 0.015, have been tested.

The theoretical model has been applied with the assumption of a singular crack tip stress field. The power law $\sigma_0(w)=\rho\sigma_u(1-w/w_c)^2$ has been assigned to describe the bridging mechanism of the steel fibers, where σ_u=169Nmm^{-2} is the maximum fiber pull-out strength and w_c is the critical crack opening displacement, equal to 12.5mm. The above law has been chosen by Jenq and Shah to represent the results of pull-out tests on single aligned fibers. The dimensionless parameters $\tilde{E}\tilde{w}_c$ and N_P, controlling the mechanical behavior, are given by $\tilde{E}\tilde{w}_c$=1147 and N_P=0, 0.27, 0.54 and 0.80, for ρ=0.00, 0.005, 0.010 and 0.015, respectively.

Fig.6.a shows the dimensionless moment-vs.-rotation diagram of the unreinforced mortar beam. The theoretical curve has been obtained by means of LEFM. Apart from the pre-peak loading phase, controlled by microcracking phenomena neglected by LEFM, and the peak value, which is greater than the real one, a good agreement is found between the two curves (see Fig.2).

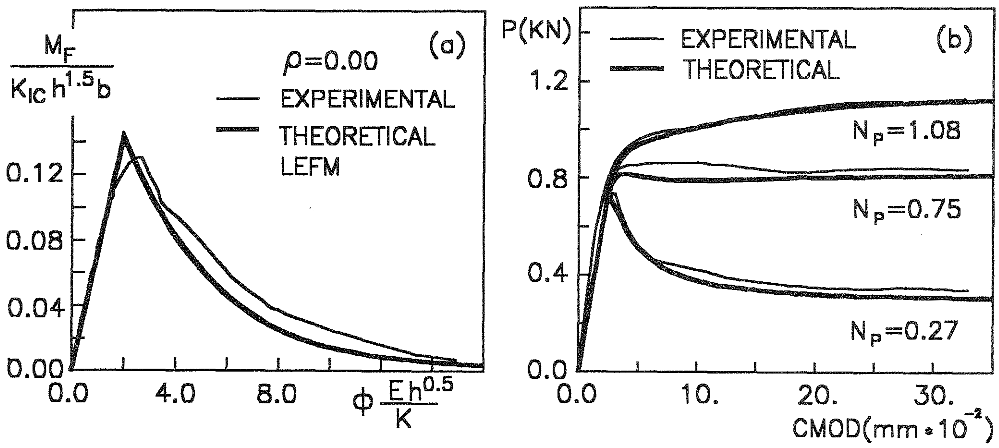

Fig.6: a) Dimensionless moment-vs.-rotation curves for a mortar beam in bending. Comparison between experimental (Jenq and Shah, 1986) and theoretical results (LEFM). b) Load-vs.-CMOD curves for fiber-reinforced mortar beams. Comparison between experimental (Jenq and Shah, 1986) and theoretical results.

In Fig. 6.b the experimental and theoretical curves, relating the applied load to the crack mouth opening displacement (CMOD), are shown for the three beams with ρ=0.005, 0.010 and 0.015. The diagram highlights a transition from a strain-softening behavior, for the beam with ρ = 0.005, to a strain-hardening behavior, for the beam with ρ = 0.15.

It is observed that the global strain–softening behavior and the hyper–strength phenomenon of the beam with $\rho = 0.005$ are faithfully reproduced by the model, and are accounted for by the low brittleness number $N_P = 0.27$. The two theoretical curves for N_P=0.75 and N_P=1.08 reproduce the behavior of the beams with $\rho = 0.01$ and $\rho = 0.015$, respectively. Note that the values of N_P are higher than those previously evaluated for the two beams, which would have led to ultimate loads lower than those experimentally determined. This discrepancy is explained by the initial assumption of a maximum pull–out load σ_u equal to the experimentally determined value for fibers pulled–out along their alignment. In actual fiber–reinforced beams the fibers are usually pulled out off–axes during crack propagation. In high fiber volume ratio beams, the above fact usually leads to an increase in the maximum pull–out load (Ouyang et al. 1994). The higher pull–out load can be accounted for by assuming a higher effective fiber volume ratio ρ_e. The discrepancies between the theoretical and the experimental values disappear on assuming $\rho_e = 0.014$ and $\rho_e = 0.020$, which leads to $N_P = 0.75$ and $N_P = 1.08$, respectively.

5 Conclusions

Some applications of a nonlinear fracture mechanics model, formulated by the authors for analysis of the flexural behavior of brittle–matrix composites, have been shown. The constitutive relationship, linking the crack–propagation moment to the localized rotation of a cracked cross section, has been evaluated based on different assumptions for the crack tip stress field, the crack growth criterion and the bridging mechanism of the secondary phases. Linear elastic fracture mechanics solutions have been used to predict the tail of the curve.

In the first application a finite stress field has been assumed in the crack tip vicinity, and the global toughening mechanism of the homogenized composite has been represented by a closing traction distribution, acting along a fictitious crack and linked to the crack opening displacement by a cohesive law. On modeling the cohesive tractions as a linearly decreasing function of the crack opening displacement, a ductile–brittle transition in the flexural response of the beam has been predicted, when the depth increases.

In the second application a singular field has been assumed at the tip of the crack, and the toughening mechanisms for the matrix and the secondary phases have been modeled by means of a critical stress intensity factor and of a distribution of closing tractions applied along the fictitious crack, respectively. On modeling the bridging tractions as a constant function of the crack opening displacement until a critical value, a double brittle–ductile–brittle scaling transition has been predicted in the flexural behavior. The beam depth beyond which the mechanical response varies from globally stable to globally unstable can be defined once the mechanical properties of the different phases, the volume ratios, and the properties of the interface are fixed.

6 References

Ballarini, R., Shah, S.P. and Keer, L.M., (1984) Crack growth in cement–based composites, **Eng. Fracture Mech.**, 20, 433–445.

Barenblatt, G.I. (1959), The formation of equilibrium cracks during brittle fracture. General ideas and hypotheses. Axially–symmetric cracks, **J. of Applied Mathematics and Mechanics**, 23, 622–636.

Barenblatt, G.I. (1962), The mathematical theory of equilibrium cracks in brittle fracture, **Advanced in Applied Mechanics**, (ed.H.L. Dryden and T. von Karman), pp. 55–129, Academic Press, New York.

Bosco, C. and Carpinteri, A.(1992), Softening and snap–through behavior of reinforced elements, **J. Engng. Mech.**, 118 (8), 1564–1577.

Bosco, C. and Carpinteri, A. (1995), Discontinuous constitutive response of brittle matrix fibrous composites, **Int. J. Mech. Phys. Solids**, 43 (2), 261–274.

Carpinteri, A. (1981), Static and energetic fracture parameters for rocks and concretes, **Materials and Structures**, 14, 151–162.

Carpinteri, A. (1984), Stability of fracturing process in r.c. beams, **J. Struct. Engng.**, 110 (3), 544–558.

Carpinteri, A. (1989), Cusp catastrophe interpretation of fracture instability, **J. Mech. Phys. Solids**, 37, 567–582.

Carpinteri, A. and Massabó, R. (1995.a), Bridged versus cohesive crack and double brittle–ductile–brittle size–scale transition in flexure, submitted to **J. Mech. Phys. Solids**.

Carpinteri, A. and Massabó, R. (1995.b), Reversal in the failure scaling transition of brittle matrix fibrous composites, submitted to **J. Engng. Mech.**.

Cotterell, B., Paramasivam, P. and Lam, K.Y. (1992), Modelling the fracture of cementitious materials, **Materials and Structures**, 25, 14–20.

Cox, B.N. and Marshall, D.B. (1994), Concepts for bridged cracks in fracture and fatigue, **Acta Metall. Mater.**, 42 (2), 341–363.

Desayi, P. and Ganesan, N. (1986), Fracture behavior of ferrocement beams, **J. Struct. Engng.**, 112 (7), 1509–1525.

Dugdale D.S. (1960), Yielding of steel sheets containing slits, **J. Mech. Phys. Solids**, 8, 100–104.

Foote, R.M.L., Mai , Y–W and Cotterell, B. (1986), Crack growth resistance curves in strain–softening materials, **J. Mech. Phys. Solids**, 34 (6), 593–607.

Jamet, D., Gettu, R., Gopalaratnam, V.S. and Aguado, A. (1995), Toughness of fiber–reinforced high–strength concrete from notched beam tests, presented at **ACI Spring Convention: Session on testing of reinforced concrete, ACI special publication**, in press.

Hillerborg, A., Mooder, M. and Petersson, P.E. (1976), Analysis of crack formation and crack growth in concrete by means of fracture mechanics and finite elements, **Cem. Conc. Research**, 6, 773–782.

Hillerborg, A. (1989), Analysis of fracture by means of the fictitious crack model, particularly for fibre reinforced concrete, **Int. J. Cement Composites**, 2 (4), 177–184.

Jenq, Y.S. and Shah, S.P. (1985), Two parameter fracture model for concrete, **J. Engng. Mech.**, 111 (10), 1227–41.

Jenq, Y.S. and Shah, S.P. (1986), Crack propagation in fiber–reinforced concrete, **J. Engng. Mech.**, 112 (1), 19–34.

Li, V.C. and Liang, E. (1986), Fracture processes in concrete and fiber reinforced cementitious composites, **J. Engng. Mech.**, 112, 566–586.

Mai, Y.W. (1985), Fracture measurements for cementitious composites, in **Application of fracture mechanics to cementitious composites**, (ed. Shah S.P.), Martinus Nijhoff Dordrecht, 399–429.

Ouyang, C., Pacios, A. and Shah, S.P. (1994), Pullout of inclined fibers from cementitious matrix, **J. Engng. Mech.**, 120 (12), 2641–2659.

Romualdi, J.P. and Batson, G.B. (1963), Behavior of reinforced concrete beams with closely spaced reinforcement, **J. of the ACI**, 60–40, 775–789.

Shah, S.P. (1988), Fracture toughness of cement–based materials, **Materials and Structures**, 21, 145–150.

Tada, H., Paris, P.C. and Irwin, G. (1985), **The Stress Analysis of Cracks Handbook**, Paris Productions Incorporated (and Del Research Corporation), St. Louis, Missouri.

Visalvanich, K. and Naaman, A.E. (1983), Fracture model for fiber reinforced concrete, **ACI J.**, 80, 128–138.

Wecharatana, M. and Shah, S.P. (1983), A model predicting fracture resistance of fiber reinforced concrete, **Cement and Concrete research**, 13, 819–829.